A 20-K, 600-W, Cryocooler-Based, Supercritical Helium Circulation System for the SPARC Toroidal Field Model Coil Program

Philip C. Michael, Theodore Golfinopoulos, Ernest Ihloff, Alexander Zhukovsky, Shane Schweiger, Vincent Fry, Colin O'Shea, Amy Watterson, Daniel Nash, Rui F. Vieira, Jeffrey Doody, Raheem Barnett, Erik A. Voirin, Larry Bartoszek, Richard F. Lations, and Zachary S. Hartwig

***Abstract*—From June 2019 to July 2021, the MIT Plasma Science and Fusion Center, in collaboration with Commonwealth Fusions Systems, designed, built, and commissioned a test facility at the Massachusetts Institute of Technology to evaluate the performance of a rare-earth-yttrium-barium-copper-oxide-based, 2.9-m tall, 1.9-m wide Toroidal Field Model Coil (TFMC) for the SPARC tokamak. This article presents the facility's supercritical helium (SHe) circulation system design and measured performance. The facility employed a forced-flow SHe circulation loop cooled by cryocoolers to provide a nominal cooling power of 600 W at 20 K and up to 70 g/s SHe flow to the TFMC at an absolute pressure of 20 bar. The reliance on cryocoolers as the facility's cooling source was an ideal arrangement. Procurement costs were modest, acquisition time was reasonable, and seating requirements were minimal. A steady improvement in cryocooler design provided a simple-to-use system with sufficient cooling capacity for our needs. Extensive, closed-loop analyses were performed both to support this procurement and to finalize the overall design of the SHe cooling circuit. The SHe system worked reliably, permitting flexible operation of the TFMC test facility under all working conditions.**

***Index Terms*—Cryocooler, high-temperature superconductor magnets, magnet test facility, supercritical helium (SHe) cooling.**

I. Introduction

THE SPARC Toroidal Field Model Coil (TFMC) Program was an approximately three-year effort between 2018 and 2021 that developed novel rare-earth yttrium barium copper oxide (REBCO) superconductor technologies [1], [2], [3], [4], and then, utilized those technologies to successfully design, build, and test a first-in-class, high-field (∼20 T) representative scale (∼3 m in linear size) superconducting toroidal field (TF) coil. With the principal objective of retiring the design, fabrication, and operational risks inherent in large-scale, no-insulation (NI) REBCO superconducting magnets for fusion energy devices, the program was executed jointly by the MIT Plasma Science and Fusion Center (PSFC) and Commonwealth Fusion Systems (CFS) as a critical technology enabler of the high-field pathway to fusion energy [5], and in particular, as a risk retirement program for the toroidal field magnet in the SPARC net-energy fusion tokamak [6]. This article is a part of a collection of papers intended to cover various aspects of the SPARC TFMC program [7], including the design and fabrication of the magnet [8], the design and assembly of the test facility [9], [10], and an overview of the results from the experimental test campaigns carried out in the fall of 2021 [11].

From the outset, high-temperature-superconductor-based (HTS) fusion magnets were designed to operate at temperatures in the range from 10 to 30 K as a means to enhance conductor stability [12]. Metal enthalpy at those temperatures increases by nearly two orders of magnitude, while conductor current density, J_e, generally decreases by less than a factor of two when compared to operation near 4 K. More recent design studies highlighted the marked improvement in refrigerator Carnot efficiency near 20 K as a means to optimize the overall system cost [13]. The SPARC toroidal field magnet, which is intentionally lightly shielded to achieve compact size, is likewise expected to operate at temperatures near 20 K. Its increased operating temperature, relative to existing superconducting tokamaks, enables SPARC to pursue a large, nuclear-heat-load design [6].

This manuscript describes the design, implementation, and operation of the supercritical helium (SHe) circulation system used to test the SPARC TFMC. Based on prior system optimization studies, the TMFC was to be cooled with SHe at nominal 20 K operating temperature. The cooling circuit's nominal operating pressure was capped at 20 bar to permit high-density, high-mass-flow-rate operation, to minimize the temperature rise through the cooling circuit and yet stay within the engineering limits of readily available cryogenic components. Unless otherwise specified the unit bar in this article refers

Manuscript received 18 August 2023; revised 23 October 2023; accepted 5 November 2023. Date of publication 13 November 2023; date of current version 7 December 2023. This work was supported by Commonwealth Fusion Systems (CFS). *(Corresponding author: Philip C. Michael.)*

Philip C. Michael, Theodore Golfinopoulos, Ernest Ihloff, Alexander Zhukovsky, Shane Schweiger, Vincent Fry, Amy Watterson, Rui F. Vieira, Jeffrey Doody, Richard F. Lations, and Zachary S. Hartwig are with the MIT Plasma Science and Fusion Center, Cambridge, MA 02139 USA (e-mail: pmichael@mit.edu; golfit@mit.edu; eihloff@mit.edu; zhukovsky@psfc.mit.edu; shaneschweiger@live.com; vfry@cfs.energy; watterson@psfc.mit.edu; rfvieira@mit.edu; doodyjw@mit.edu; lations@psfc.mit.edu; hartwig@mit.edu).

Colin O'Shea, Daniel Nash, and Raheem Barnett are with Commonwealth Fusion Systems, Cambridge, MA 02139 USA (e-mail: colinposhea@gmail.com; daniel@nashfamily.net; raheem@cfs.energy).

Erik A. Voirin is with eVoirin Engineering Consulting, North Aurora, IL 60542 USA (e-mail: erikvoirin@gmail.com).

Larry Bartoszek is with Bartoszek Engineering, Aurora, IL 60506 USA (e-mail: design@bartoszekeng.com).

Color versions of one or more figures in this article are available at https://doi.org/10.1109/TASC.2023.3332266.

Digital Object Identifier 10.1109/TASC.2023.3332266

TABLE I
DESIGN PARAMETERS FOR THE SPARC-TFMC

Parameter	Value
Numbers of pancakes x turns per pancake	16 x 16
Magnet inductance, L_m	0.136 H
Total turn–turn resistance, R_m	11 $\mu\Omega$
Pancake-pancake joint resistance, R_j	3 nΩ (each)
Nominal terminal current, I_{op}	40.5 kA
Stored magnetic energy at I_{op}	110 MJ
Winding pack mass	5113 kg
Overall magnet mass (including case)	10,058 kg
Magnet width and length	1.9 m x 2.9 m
Coolant type	SHe
Nominal coolant pressure and temperature	20 bar, 20 K
Helium volume in winding pack	0.032 m^3
Helium volume per inlet and outlet plenum	0.153 m^3

to an absolute pressure measurement, while bar-g refers to gauge pressure.

The rest of this article is organized as follows. Section II of this manuscript discusses the selection of the SHe cooling scheme developed for the TFMC, while Section III presents its chosen implementation. Section IV discusses the interplay between the designs of the TFMC and the TFMC test facility as they impact specific features of the cooling scheme. The performance of the SHe cooling system during the TFMC test program is presented in Section V. Finally, Section VI concludes this article.

II. COOLING SYSTEM ARCHITECTURE

A. TFMC Cooling Requirements

The design of the TFMC test facility began in earnest during July 2019. By that time the basic design of the TFMC had been determined. In brief, the TFMC employed a novel no-insulation, no-twist (NINT) cable-in-plate architecture [4]. The initial TFMC design contained 14 (later increased to 16) D-shaped NINT pancakes, each consisting of 16 conductor turns per plate. The pancakes were alternately joined at their inner and outer diameters, respectively, with joints to terminal end plates at the outer diameters of the outermost pancakes in the stack. Table I summarizes the design parameters for the TFMC.

Cooling for adjacent TFMC pancakes was provided by machining grooves into each pancake on the opposite sides of the plate from the conductor turns. The cooling grooves machined into one pancake were used to cool the conductor turns in its neighbor. Each cooling groove was split into two halves, one following the straight leg of the D and the other following the curved leg, resulting in a total of 528 cooling paths in all once dedicated joint cooling paths were added. The cooling scheme was selected to emulate that anticipated for the SPARC TF magnets, which are only lightly shielded and subject to strong nuclear heating, especially along the TF magnets' innermost turns [6]. A complete description of the TFMC design is presented in [8].

The anticipated charging behavior for an NINT-based TFMC is the same as that previously presented for single-tape-wound NI magnets [14], [15]. The charging characteristics are governed by the total magnet inductance, L_m, and turn–turn resistance, R_m, which for the as-built TFMC were nominally 136 mH and 11 $\mu\Omega$, respectively, yielding an L_m/R_m time constant of roughly 12 400 s. To limit the inlet to outlet temperature rise due to turn–turn (radial-current-flow) heating of the TFMC to nominally less than 1 K during charging, the facility was designed to charge the magnet linearly from zero to a terminal current, $I_{\rm op}$, of 40.5 kA within 24 h (86 400 s) duration. The ratio of the TFMC's relatively long charging duration, t_d, to its $L_m/R_{\rm m}$ time constant places it in a slow charging regime, for which the asymptotic, turn–turn power dissipation, $P_{\rm tt}$, can be approximated as

$$P_{\rm tt} = (L_m\, I_{\rm op})^2/\left(R_m\, t_d^2\right)\,[15]\,. \tag{1}$$

In addition to turn–turn heating during charging, the magnet is also subject to resistive heating at the pancake-to-pancake and terminal joints. Assuming a total of 19 joints, n_j, inside the TMFC (15 between pancakes, two to the terminal plates, and two from the terminal plates to the magnet terminals), each having a nominal joint resistance, R_j, of 3 nΩ, adds an additional $n_j\ I_{\rm op}^2\ R_j$ of joint resistance heating to the magnet's cooling circuit toward the end of the current upramp.

The TFMC's anticipated electrical characteristics and proposed charging sequence yielded a nominal, peak heat load of roughly 465 W (370 W of turn–turn dissipation and 95 W of joint resistance heating), to be removed using 20 bar, 20-K helium, requiring a mass flow rate of about 70 g/s to maintain roughly 1-K inlet-to-outlet temperature difference. Combining the TFMC heat loads with the estimated 62-W heat load from the facility current leads (CLs) and cold bus (discussed in Section IV-D) and 10–20 W from gravity supports, thermal radiation, and residual gas heat loads, indicated a need for between 500 and 600 W cooling capacity at 20 K to support the test plan objectives.

B. Cooling System Down Selection

At the time the TFMC test facility design began, the PSFC retained a large liquid nitrogen (LN2) infrastructure that was developed to support operation of the Alcator C-Mod tokamak [16]. This infrastructure included an 18 000-gal (68000 L) LN2 storage tank and vacuum jacketed piping extending into the TFMC test hall. The cryogenic helium infrastructure required for the TFMC test facility needed to be developed from scratch.

Preliminary assessment of the test facility's cryogenic infrastructure followed established historic precedent—to employ LN2 to cool cryostat radiation shields, and a large capacity helium refrigerator/liquefier to cool the facility CLs and magnet circuit [17], [18], [19], [20], [21], [22]. Fig. 1 shows the general arrangement for this scheme. The arrangement assumed the use of conventional, liquid helium (LHe)-cooled CLs optimized for 50-kA operation and an internal SHe loop operating at moderate pressure for cooling the TFMC, coupled through a heat exchanger to a high-capacity cryogenic cooling source. This arrangement effectively decouples both the cooling loop pressure and instantaneous heat load from the cooling source, permitting relatively independent optimization of both.

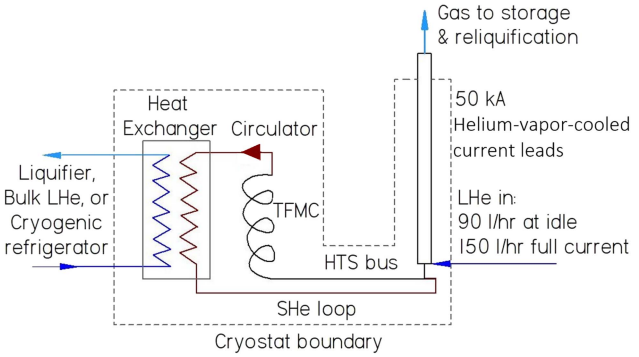

Fig. 1. Conventional facility cooling arrangement employing a closed circulation loop for the magnet under test, with LHe or helium gas cooling of the current leads.

CLs of 50 kA were selected to permit potential overcurrent operation of the TFMC, which was under consideration at the time. From [23], a pair of 50-kA LHe-cooled leads nominally consume 90 L/h of LHe at idle, and 150 L/h during full current operation. The initial scoping study also assumed: use of atmospheric-boiling LHe as the primary cooling source for the TFMC cooling loop, complete transfer of the total enthalpy available from boiling to 20-K gas in the heat exchanger, and zero heat load from the circulator pump. This idealized heat exchanger requires an additional 120 L/h of LHe to produce the target TFMC cooling power toward the end of the current upramp. The combined total of roughly 240-L/h LHe consumption for both TFMC and CL cooling far exceeds the total capacity of the nearby MIT cryoplant.

Three LHe-based cooling options were briefly considered. One was the construction of an LHe plant dedicated solely to the TFMC facility. Another required the acquisition of one or more 10 000–30000-L LHe storage dewars, which would be used to accumulate the total production from the MIT LHe plant over a number of weeks leading up to the test. The last, would be to procure and work from an LHe tanker truck placed in close proximity to the test facility. All three options would also require the acquisition of a significant LHe-distribution and helium gas recovery and storage infrastructure. Hence, LHe-based cooling was deemed not feasible given the limited physical size of the test facility, the significant increase in program scope, and the risk of a significant schedule delay. In addition, due to on-going supply shortages, our helium supplier indicated that it was highly unlikely that they could deliver the quantities of helium required for any of these options within our requested time frame.

After exhausting a variety of alternative schemes, we decided to add the design of a pair of LN2-cooled, 50-kA-capacity hybrid CLs with REBCO-based low-end sections to the program scope and to limit the use of helium in the TFMC cooling loop only where its use is unavoidable.

The design, construction, and operation of the LN2-cooled CLs is presented in [10]. The incorporation of LN2-cooled CL in the facility adds roughly 62-W heat load to the SHe circuit to support both the cold bus joints, which had to be extended to locate the CLs' REBCO sections in a low-fringe-magnetic-field area and for cooling the low-temperature ends of the leads. By placing the cold bus and REBCO lead sections in parallel with return flow from the TFMC and allowing them to operate a few degrees warmer, there was no need to increase the total mass flow rate through the SHe cooling loop.

III. TFMC Test Facility's Helium Cryoplant

A. Cryocooler-Based Cryocirculator Modules

The cooling capacities of cryocooler-based 20-K helium circulation loops have increased steadily during the past several years [24], [25], [26], [27], [28], [29], [30], [31]. Because of their ease of operation, these systems are ideal for intermittent operation by relatively small, moderately trained cryogenic groups like ours.

In October 2019, we contracted Absolut System of Seyssinet, France, for the design and construction, within one year, of a cryocooler-based helium circulation system capable of providing at least 500 W of cooling power when operated with 20-bar, 20-K helium at a nominal mass flow rate in the range between 50 and 100 g/s.

To support the design process, Absolut System performed several full-circuit thermohydraulic analyses of the proposed TFMC cooling loop. These analyses examined the design and arrangement of their cold head heat exchangers; the cold head cooling capacities; performance characteristics for their cryocirculator fans; preliminary designs for the transfer lines from their system to and from the TFMC; the size and mass of the TFMC; the sizes and numbers of TFMC pancake cooling channels; and the heat loads summarized previously. Both cooldown and routine operation simulations were performed, both showing acceptable performance.

Fig. 2 shows the arrangement of the delivered system. For ease of assembly, transportation, and operation, the system consists of two, near-identical cryomodules. Because both cryocirculator fans spin in the same direction, the cryomodules are mirrored to permit proper orientation of their supply and return ports when they are connected together in parallel.

Each cryomodule contains four Cryomech AL630 single-stage cold heads. Each cold head was modified to incorporate a gas heat exchanger directly into the cold head stage, rather than mounting a separate heat exchanger to the cold head after manufacturing. This eliminates any uncertainty regarding the thermal contact between the heat exchanger and the cooling stage. The cold heads are arranged in a 2×2 series–parallel configuration, which yielded best combination of cooling power and mass flow rate during the 20-bar, 20-K thermohydraulic simulations.

In Fig. 2, the cryomodule 1 cold heads are denoted as CH1 through CH4, while those in cryomodule 2 are denoted as CH5 through CH8. The Cernox sensors measuring the temperatures of the supply, or outlet, helium are denoted as TT1 and TT8, respectively, while those measuring the temperatures of the return flows are denoted as TT2 and TT9. The Cernox sensors measuring the temperatures at the tips of cold heads CH1 through CH4 are denoted as TT3 through TT6, while those measuring cold heads CH5 through CH8 are denoted as TT10 through TT13. Platinum RTDs TT7 and TT14 (not shown), respectively,

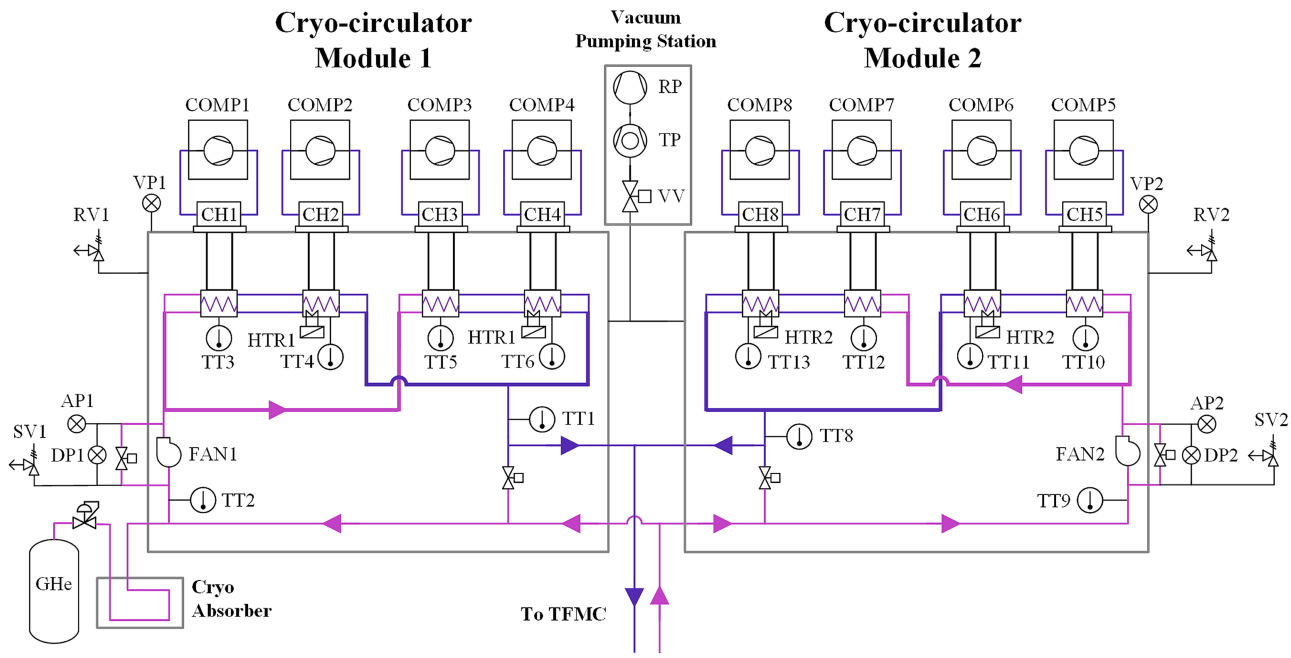

Fig. 2. Arrangement of the cryocirculator modules.

monitor the temperatures at the top plates of the cryomodules' radiation shields.

The cold head compressors can be remotely activated and monitored from the test facility control room to permit large-scale changes in the cryomodules' cooling power, such as during the initial stage of facility cooldown. Each cryomodule is also equipped with an Absolut System cryocirculator fan, capable of operating at rotation speeds ranging from 15 to 60 kr/min, with maximum speed in the cold condition limited by motor torque of not more than 24 mN·m. Based on the thermohydraulic modeling, the fans are placed between the return helium port and the first pair of cold heads in each cryomodule. The compressed, ambient temperature helium gas needed to build and maintain circuit pressure during cooldown is similarly injected between the return helium ports and the fans. Our fans were equipped with titanium housing to minimize conduction to the cold environment. The cryocirculator fans can also be activated, controlled, and monitored from the control room.

The fan performance is well characterized and was used to estimate helium mass flow through the fans in the absence of dedicated flow meters. The differential pressure sensors used to measure the pressure rise through the fans are denoted as DP1 and DP2, respectively, in Fig. 2, while the sensors used to measure the absolute pressures at the fan outlets are denoted as AP1 and AP2. Both the helium circuit and the vacuum space for each cryomodule are equipped with overpressure relief valves to limit pressure build-up during off-normal events. The helium circuit relief valves are designed to open at 26 bar-g, while the vacuum space valves nominally open at 0.2 bar-g.

To permit stand-alone performance testing, such as during factory and acceptance test upon receipt, each cryomodule is equipped with a bypass valve between its supply and return ports. The final pair of cold heads in each cryomodule are equipped with feedback-temperature-controlled heaters, which were used

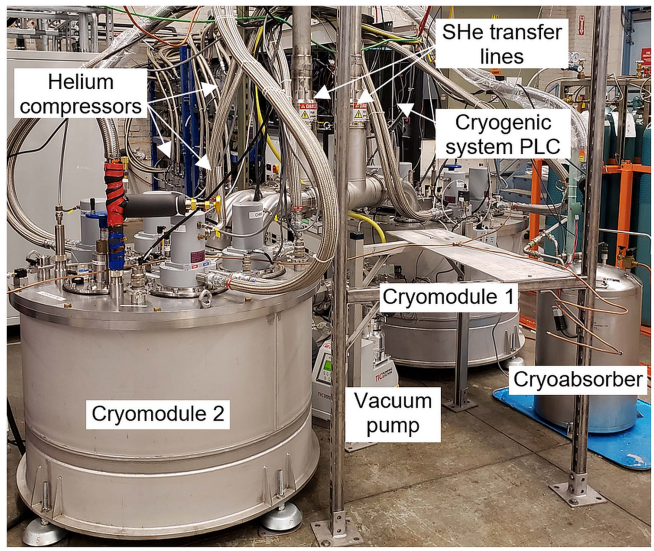

Fig. 3. Digital image of SHe cryomodules installed in the TFMC test facility.

to verify system performance during acceptance testing and to trim the supply temperature during test of the TMFC. The cryostat for each cryomodule has a diameter of 1.2 m and a height of 0.8 m. Fig. 3 shows a digital image of the SHe circulation system installed within the TFMC test facility.

B. Acceptance Testing of the Cryomodules

Although the first Absolut System cryomodule was received at MIT in September 2020, we did not complete its incoming acceptance test until December 2020 due to both component installation and assembly and on-going and continuing site preparations needed to support the test. The second cryomodule

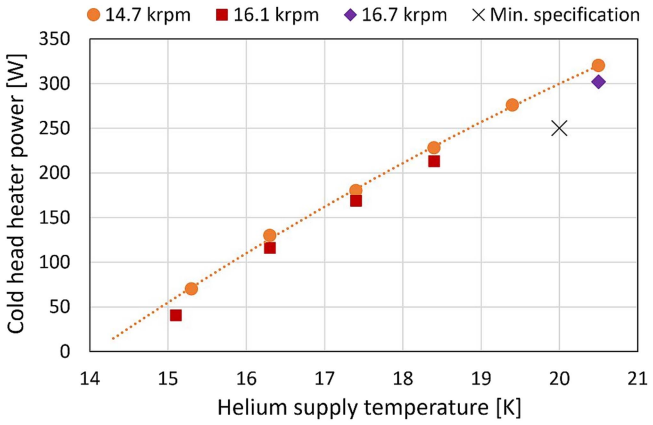

Fig. 4. Cold head heater power (cooling capacity) versus helium supply temperature during acceptance testing of the second cryocirculator module at various fan speeds, showing small reduction in cooling capacity with increasing fan speed.

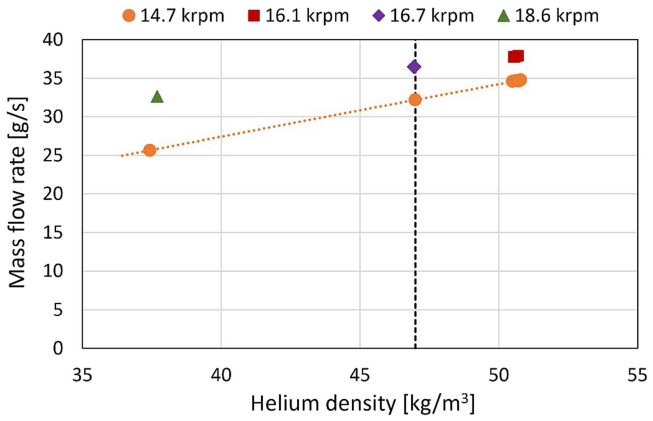

Fig. 5. SHe mass flow rate versus density at various cryocirculator fan speeds. The vertical dashed line shows the helium density at the system's nominal 20-K, 20-bar operating point.

was received at MIT in November 2020 and passed its acceptance test during January 2021.

To perform a cryomodule acceptance test, the supply and return ports were plugged and the corresponding vacuum ports were covered. The cryostat was then evacuated to below 10^{-5} torr or better, using a small turbopump station, which remained active through the test. The bypass valve between the supply and return ports was opened to permit helium circulation within the cryomodule and the cryocirculator fan was energized. Compressed, Grade-5 helium gas was supplied to the cryomodule's gas inlet port, without precooling. The cold heads were switched ON in sequence starting with a single cold head at time zero, adding a second cold head as the circuit temperature passed below 120 K, and the remaining two as the circuit stabilized to its base temperature roughly 4 h after the start of cooling. As the circuit cooled, the vacuum pressure in the cryostat dropped by nearly two orders of magnitude.

Figs. 4 and 5 show performance data from the acceptance test of the second cryomodule. The first cryomodule showed near identical performance over the range of operating conditions examined. Although the helium density during the second cryomodule's acceptance test was generally 50 kg/m^3, a few tests were performed at both 37 and 47 kg/m^3 for comparison. The circuit pressure during the tests ranged from 15 to 22 bar as the feedback-controlled helium supply temperature was actively varied between 15.0 and 20.5 K to determine the total cold head heating power needed to achieve each supply temperature. It generally took about 15 min for the heater power to stabilize each time the setpoint temperature was changed. A few different fan speeds were investigated from the minimal achievable speed of 14.7 kr/min to the maximum (which varies with density) allowed by the fan motor's continuous torque rating of 24 mN·m.

The cold head heater power versus helium supply temperature data presented in Fig. 4 were taken as a measure of the cooling capacity the cryomodule can provide when the module is connected to the test facility. The dashed line in Fig. 4 shows a quadratic fit of the heating power versus supply temperature at the minimum fan speed of 14.7 kr/min. The decrease in heating power with increasing fan speed is attributed to the increased shaft work, which due to inevitable fan inefficiency also adds heating to the helium circuit. The acceptance results indicate that each cryomodule can provide at least 300 W of cooling power at 20 K (600 W combined) significantly above the minimum target specified in their procurement, which is indicated by the black X in Fig. 4.

The circulator fan in each cryomodules exhibits a monotonic relation between its volumetric flow rate, Q_i, and the differential pressure across the fan, DP_i. In parameterized form, this relation holds across a wide range of fluid density, ρ_i, and rotational speed, ω_i. The parameterized flow coefficient $Q_c$equals Q_i/ω_i, while the pressure coefficient P_c equals $\mathrm{DP}_i/(\rho_i\omega_i^2)$.

Fig. 5 shows the variation in computed mass flow rate versus the helium density at the cryocirculator fan. The mass flow rate for each module, $\dot{m}_i$, was computed as the product of the helium density at the fan inlet, $\rho_i(\mathrm{AP}_i, T_i)$, times the volumetric flow rate through the fan, Q_i, where AP_i is the absolute pressure at the fan and T_i is the helium temperature at the fan inlet. The volumetric flow rate, in turn, was computed from the manufacturer-provided fan curve ($Q_c = f(P_c)$), the differential pressure across the fan, DP_i, and its rotational speed ω_i, as

$$\dot{m}_i = \rho_i\,(\mathrm{AP}_i,\ T_i)\ Q_i\,(\omega_i, \mathrm{DP}_i,\ \rho_i)\,. \tag{2}$$

Fig. 5 shows the expected trend that for a system with fixed hydraulic impedance, the mass flow rate at a fixed temperature and pressure is set chiefly by the cryofan's rotational speed. Because the hydraulic impedances of TFMC and its associated interconnect piping were significantly smaller than the internal impedance of the cryomodules, we reasonably expected to achieve nominal mass flow rates from each module during the TFMC test campaign in the range from 30 to 35 g/s (60 to 70 g/s combined) at the proposed 20-bar, 20-K operating point, where the helium density is 47 kg/m^3. This density is indicated by the black dashed vertical line in Fig. 5.

C. *Use of LN2 Trace Lines for Cryomodule Radiation Shields*

During the incoming acceptance tests of each cryomodule, we experienced significant difficulty to precisely regulate LN2

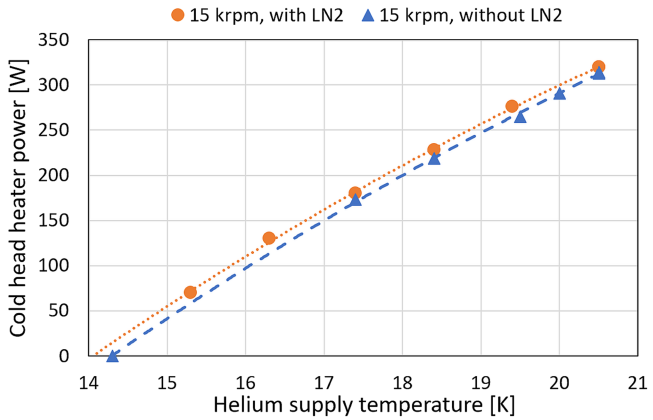

Fig. 6. Cold head heater power versus supply temperature at 15 kr/min fan speed with, and without the use of LN2 cooling for the module's thermal radiation shield, showing a loss in cooling capacity of roughly 10 W at a supply temperature of 20 K.

flow passing through the rather short trace line embedded in each module's upper radiation shield plate. Either the trace line would run mostly dry over time, resulting in gradual warming of the shield, or we had liquid venting through the trace lines' exhaust ports, which risked freezing and breaking the o-rings that secured the LN2-ports to the cryostat cover plate. This behavior was exacerbated by intermittent use of the test hall's LN2 distribution circuit for other uses.

Fig. 6 presents results from a follow-on test of the second cryomodule, which sought to assess the impact on the module's cooling capacity if we were to forego active cooling of the shield. As before, Fig. 6 plots the temperature-controlled cold head heater power versus the module's helium supply temperature. The helium densities during these tests ranged from 25 to 47 kg/m^3 as the nominal circuit pressures in the helium circuit ranged from 12 to 20 bar. The results show a loss of roughly 10 W of cooling power at 20 K when the shields are not actively cooled, which is a small price to pay for significantly simpler operation. Our decision was to not use LN2 cooling for the shields. If we had to design the system again, we would opt instead for the use of a small, 80-K cryocooler for this purpose.

IV. System Integration

The concurrent design, construction, and commissioning of the TFMC [8], 50-kA CL [10], helium circulation system, and overall TFMC test facility [9] by relatively small teams with significantly overlapping membership permitted design challenges for one program element to be alleviated by relatively minor modification to the remaining program elements. A wide range of thermohydraulic analyses were used to support these decisions. The simplest models were implemented in MATLAB [32], with subroutine calls to REFPROP [33]. Subscale models were typically implemented in Ansys-Fluent [34], while full, closed-circuit models were implemented in MathWorks Simscape [35]. This section briefly summarizes a few of those interactions as they relate to the as-built implementation of the test facility's SHe cooling loop. The effect of the tradeoffs on the other program elements is summarized in the respective companion articles.

A. TFMC Case as Pressure Boundary

The decision to cool the TFMC winding pack using grooves machined into the backs of the NINT pancakes required that the magnet case act as a helium pressure boundary. Mechanical analyses were needed to examine not only the transfer of electromagnetic loads to the case but also the case's leak tight performance subject to anticipated pressure peaking during quench. The use of the magnet case as a pressure boundary also required 1000 lead wires for the winding pack's embedded instrumentation to be extracted through the helium pressure boundary [8].

Rather than extracting the instrumentation lead wires directly through the sidewall of the case, where the feedthrough pins would need to reliably seal against 20-bar, 20-K SHe, we chose instead to route the lead wires through a pair of conduits passing through and thermally anchored to the cryostat's LN2-cooled radiation shield, before exiting the cryostat via ambient-temperature feedthroughs mounted to one of the cryostat's sidewall vacuum ports. This scheme is similar to that reported for the supercritical helium cooled LHC accelerator ring [36]. Because the lead-wire conduit was oriented in a horizontal direction between the magnet case and the feedthrough ports, we developed baffles using spray foam insulation [37] to effectively reduce, to very low level, the convective heat transfer that would have otherwise occurred for the stagnant helium captured in the conduit between the magnet case and shield.

The relatively large inlet and outlet plena mounted at either end of the magnet case served several functions. These are described more fully in [8]. Although the primary function of the inlet plenum was to facilitate the assembly of the 600-mm-long joints between the magnet terminals and the winding pack terminal plates, placement of these joints in the inlet plenum also ensure that they were well cooled by the incoming helium stream. Ansys-FLUENT modeling showed that the large plena volume and resulting very-low-helium-flow velocity inside the plena provide near uniform pressure fronts at the inlet and outlet of the TFMC winding pack, and that uniform flow in the pancake cooling channels could be achieved by simply injecting and extracting helium flow toward the far ends of the plena with the helium ports oriented perpendicular to the plena axes. The flow is uniform to the extent that the mass flow rate through each channel is determined by its cross-sectional area rather than its location in the winding pack. Select channels, such as those dedicated to the pancake–pancake joints were slightly larger than average to ensure adequate cooling during steady-state operation of the TFMC.

B. Elimination of Independent Case Cooling Circuit

Historically, most SHe-cooled toroidal field magnets have used separate cooling circuits for the magnet winding pack and for the magnet case [18], [38], [39]. The case cooling circuit typically consists of parallel tube sections welded to the case in parallel, or grooves machined in to the magnet case, and

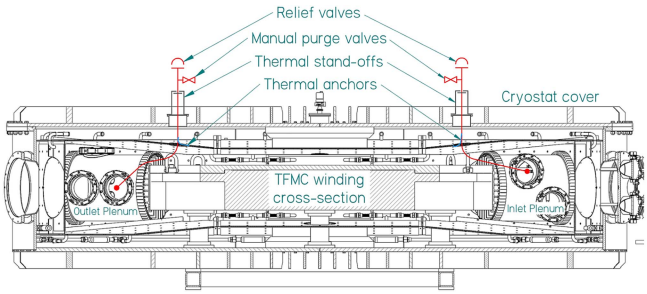

Fig. 7. Relief line routing overlaid on cryostat section drawing.

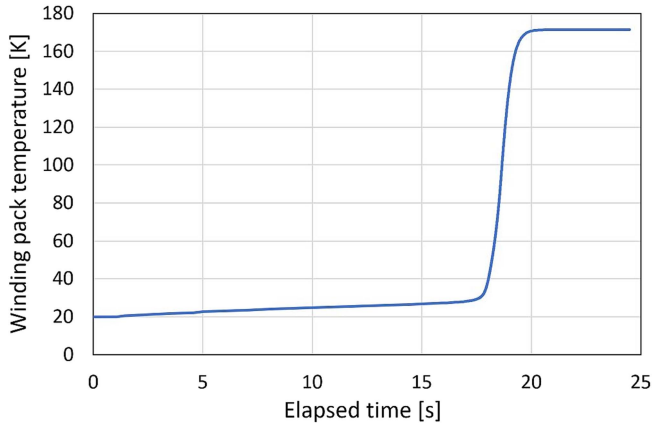

Fig. 8. TFMC winding pack temperature versus elapsed time for a 40.5-kA TFMC quench simulation starting from 20 K.

subsequently, finished with welded cover plates. To accelerate schedule, simplify case manufacture and SHe circuit topology, and reduce control system complexity, we pursued a different route by eliminating a separate case-cooling loop from our SHe circuit.

The TFMC contains relatively thick G-11CR plates placed between the broad faces of the winding pack and case. These plates accommodate winding tolerances during pancake stacking and electrically insulate the surfaces from one another. Our closed-loop Simscape model of the cooling circuit showed that by diverting roughly 10% of the total helium mass flow through cooling grooves machined into the outward facing surfaces of the G-11CR plates, the TFMC winding pack and case could be cooled together from room temperature to 20 K within five days, while maintaining maximum temperature difference between any two points in the TFMC below 50 K throughout the cool-down. Despite the slight loss in winding pack cooling capacity during current ramping, this scheme was adopted to compress the overall program (TFMC plus test facility) completion schedule.

C. Overpressure Relief

Although NI magnets are generally considered fault tolerant [14], [40], [41], there are several off-normal events, such as loss of cryostat vacuum or a fault in the magnet current supply that could potentially cause the TFMC to quench. In fact, a key component of the test program was to intentionally quench the TFMC, albeit at slightly reduced current, to characterize its quench response [11]. If a significant fault were to occur during the 40.5-kA operation of the TFMC, the TFMC's entire 110 MJ of stored magnetic energy would be dissipated within the helium circuit boundary, leading to significant risk of over-pressure damage if the pressure build-up was not mitigated by the use of a properly sized relief system.

Fig. 7 shows a section view of the TFMC in its test cryostat. The proposed routing of the overpressure relief lines, one from the inlet plenum and one from the outlet plenum, is shown in red overlay. The sizing and routing of the relief lines and relief valves were determined by coupled thermohydraulic analyses.

To limit convective heat loss in the stagnant helium in the relief lines during normal operation, the lines were oriented inclined and vertically upward, requiring them to pass through thermal anchors at the cryostat's radiation shield before exiting through the cryostat lid. Unlike the instrumentation conduit, the relief lines need to remain completely clear to function efficiently. Each relief line has a 47-mm ID and is nominally around 2-m-long, including an approximately 0.5-m long flex section to accommodate minor discrepancies in the relative positions of the TFMC and cryostat components, and thermal contraction shrinkage during cooldown.

Thermal modeling was performed first. Fig. 8 shows the results of a preliminary TFMC quench simulation, starting from steady operation at 40.5 kA current and 20 K magnet temperature. The simulation assumes a current supply fault at time zero that abruptly drives the terminal current to zero, resulting in uniform heating of the winding pack. The average temperature rise versus elapsed time follows a pattern typically observed for NI magnets [40]. The initial temperature rise occurs gradually as the magnet's azimuthal current returns through the turn–turn resistances, gradually warming the magnet toward its superconducting transition temperature. This "incubation" period is followed by a much more abrupt temperature rise as the conductor turns go normal in rapid succession. Because the helium mass constitutes less than 0.05% of the total winding pack, it has negligible impact on the computed temperature rise.

The thermohydraulic portion of the simulation considered a variety of relief line configurations and valves. Transient, 1-D modeling was performed using ANSYS CFX [42], and a real gas properties (.rgp) file generated using the helium.fld fluid file from the NIST REFPROP program. The .rpg file contained a table of all relevant SHe fluid properties over a specified range of input pressures and temperatures.

The CFX model included heat load equations, specifically, the Dittus–Boelter correlation for the heat load on the helium in the winding pack and between the relieving helium and the initially warm outlet piping. The heat load due to an assumed, simultaneous loss of cryostat vacuum was applied directly to the helium as a volumetric source term. Momentum loss source equations were used to simulate the pressure drop for helium flowing through the system. The relief valve capacity was computed and applied directly using local instantaneous fluid properties and the pressure at the inlet to the valve. The governing equations for compressible fluid flow through an orifice were used, along

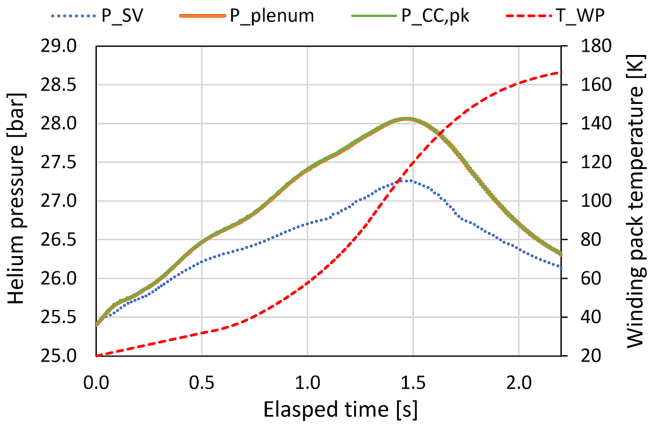

Fig. 9. Simulated relief pressure versus elapsed time for the condensed quench temperature evolution model, shown by the dashed red line. The simulated pressure starts just below the relief valves' 25.5-bar opening pressure. The simulated peak pressures in the winding pack and plena are just slightly over 28 bar.

with the proposed relief value's Code stamped orifice area and discharge capacity. The CFX model transiently solved the resulting pressure, temperature, and flow of the helium, including pressure drop effects from flow through the winding pack and the relief outlet lines.

The simulations showed a strong preference for the use of two relief lines, symmetrically placed with one to each side of the winding pack. This limits the passage of cold helium back through the warm winding pack, which would add additional heat to the helium from the winding pack cooling channels, which, as previously shown, can reach a temperature of around 170 K during a full-current quench event. The use of redundant valves also provides two parallel paths from the plena to the relief valves, reducing the pressure drop from them to the relief valves, and overall pressure build-up in the system. Due to the symmetric design of the relief system only half of the system and one of the two identical relief valves had to be simulated.

Due to an accounting oversight, the simulation included only the 0.34-m^3 helium volume contained within the TFMC winding pack and plena. The ~0.12-m^3 circuit volume contained in the cryomodules and transfer lines was inadvertently overlooked; this additional volume would have slightly slowed pressure build-up.

The simulated heat loads included: loss of vacuum to uninsulated surfaces in the plena and vent lines (38 kW/m^2), quench heat load from the winding pack, and heat from the vent lines, which initially begin with a temperature gradient along their lengths, from 20 K up to ambient temperature. Fig. 9 shows the simulated helium pressure versus elapsed time behavior during a simultaneous loss of vacuum and magnet quench event. For sake of computational efficiency, the winding pack temperature, T_WP, (dashed red line) during initial 17.8 s of the simulated quench in Fig. 8 were condensed to 0.5 s in Fig. 9. This explains the difference in elapsed time scales between the two plots.

In Fig. 9, the peak pressures in the winding pack cooling channels P_CC,pk (green line) and plena P_Plenum (thick orange line) were nearly identical due to the very low pressure drop through the winding pack. The pressure at the relief valve inlet P_SV (dotted blue line) is of course lower due to pressure drop through the relief lines. The simulation used an initial helium circuit pressure of 25.4 bar, just below the 25.5-bar valve opening pressure and an initial temperature of 20 K. These initial conditions simulate a worst-case scenario where all quench heat is dumped into the helium during the relief event, and none is used to bring pressure from operational up to the relief pressure.

The simulation indicates that the two identical Rockwell–Swendeman RSXO relief valves selected for this application, with 0.628 in^2 orifice size (Cd = 0.602) and 25.5 bar opening pressure, would effectively limit the peak pressure anywhere in the helium circuit to 28 bar in event of worst-case relief condition. The relief system is fully compliant with ASME pressure vessel code for overpressure protection, which, given the 28 bar MAWP and 16% overpressure allowance for multiple relief valves, would allow up to 32.5 bar of pressure during a relief event. Given the design margins built into the helium circuit and TFMC components, this arrangement was deemed suitable for safe operation of the TFMC.

D. Fringe Magnetic Field Accommodation

Several components on the Absolut System cryostats—pressure transducers, vacuum gauges, cold head valve motors, vacuum pumping station, and especially the high-speed cryofans—are sensitive to fringe the magnetic field. To limit the magnetic field exposure on these components, the cryostats (as well as all facility control and monitoring PLCs and data collection components) were placed just beyond the TFMC's full-field, 30-G field line, 9 m from the center of the magnet cryostat. To minimize the pressure drop through the 10.5-m-long, vacuum-jacketed helium transfer lines that connect the cryocirculator system to the magnet cryostat, we contracted PHPK Technologies to fabricate 43.5-mm ID, 30-bar pressure-rated transfer lines for our application. For 20-bar, 20-K helium at 65 g/s, the computed pressure drop through each transfer line is roughly 70 Pa. The extra transfer line length is needed to route the lines up and over one of the main access corridors in the test hall. Because we are operating so far down to the lower right of the system's fan curves, doubling the pressure drop in the entire cooling loop (TFMC, transfer lines and cryomodules) relative to that within the cryomodules only, would only decrease the available mass flow by slightly over 10%.

The transfer lines contain the only other pair of valves in the SHe cooling loop. The transfer line shutoff valves permit the magnet portion of the cooling loop to be opened to atmosphere for TFMC installation and removal, while preserving high purity gas environment in the cold head heat exchanger portion of the loop. The helium distribution lines within the magnet cryostat were designed with a 38-mm ID for a similar reason. Maintaining a low pressure drop through the helium circuit maximizes flow through the cryofans, which limits the temperature rise through the TFMC at a given heat load.

During the design of the TFMC CLs, we determined that the number of REBCO tapes needed for the HTS lead sections decreased rapidly as the CLs were moved to the lower

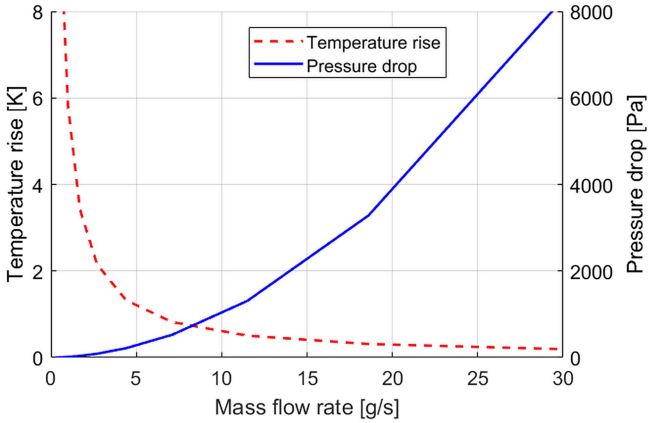

Fig. 10. Results from a parametric survey, showing temperature rise versus mass flow rate on the left-hand axis, and cold bus pressure drop versus mass flow rate on the right, with reasonable tradeoff between the two from 5 to 10 g/s mass flow rate.

fringe magnetic field, further from the magnet cryostat [10]. The required tape quantity quickly plateaued as the distance from the center of the lead pair reached 4 m from the center of the TFMC. Placement of the leads at this location required the use of approximately 3.5-m-long cold buses to reach from the TFMC terminals to the CLs. Each cold bus was formed using a modified version of MIT's VIPER REBCO cable [1] with the center cooling channel enlarged to 10 mm to reduce the SHe-flow pressure drop.

Heat loads from the TFMC terminal joints at one end of the cold bus, CL terminal joints at the other, and thermal conduction down the REBCO CL lead sections all need to be cooled by helium flowing through the cold bus cooling channels. At 40.5 kA, the nominal 3-nΩ joints at both ends of the cold bus produce a roughly 10-W heat load on the cold bus. The estimated joint resistance values were scaled from VIPER cable test results obtained at the SULTAN facility [1]. The estimated resistive heating within each CL terminal is 15 W, while the thermal conduction down the REBCO sections adds another 6 W, yielding a total estimated heat load on each cold bus of roughly 31 W.

Fig. 10 shows results from a parametric survey, showing temperature rise versus 20-K, 20-bar helium mass flow rate through each cold bus on the left-hand axis and pressure drop versus mass flow rate through the cold bus on the right-hand axis. The results show a reasonable tradeoff between pressure drop (below 1 kPa) and temperature rise (below 1 K) for cold bus mass flow rates in the range from to 10 g/s.

Because the cold bus was designed to a critical current about 60% above that anticipated for the TFMC, it can safely operate over a much broader temperature range. Thus, it is perfectly adequate to cool the bus using the TFMC's return helium flow. To satisfy the cold bus cooling loads without requiring rather long-lead-time flow control valves, or unduly restricting the total mass flow to the TFMC, we decided to split the return flow three ways, using one path for each cold bus, and a bypass line containing the bulk of the flow. To ensure sufficient cooling of the cold bus (in the 5$\sim$10 g/s range), we installed a flow control orifice in the bypass line, with orifice size designed using our Simscape model for the helium circuit. Based on the modeling, the orifice diameter was set to 14.0 mm diameter, yielding roughly 60 g/s total mass flow through the TFMC, 10 g/s mass flow through each cold bus, and less than 1 kPa pressure drop across the orifice. This was the final element needed to complete the TFMC helium circuit. The orifice plate was machined during May 2021, welded into the helium return manifold, and installed in the magnet cryostat during July 2021.

E. TFMC Helium Circuit

Fig. 11 shows a schematic arrangement of the helium circuit used during the test of the SPARC TFMC. The cryocirculator modules, connected in parallel, are shown on the lower right-hand side of the figure. During testing, the bypass valve in each module was fully closed, to ensure maximal flow to the TFMC. The cryomodules are connected by vacuum-jacketed transfer lines (described in Section IV-D) to feed-through ports on the magnet cryostat close to the TFMC's inlet plenum. The evacuated and sealed transfer lines also isolate the cryomodule vacuum from that in the magnet and CL cryostats.

The supply transfer line is connected, within the magnet cryostat, to the TFMC inlet plenum by a 1-m-long, 38-mm ID, reinforced flexible bellows, using an NW40 CeFix flange at each end. Helium enters normal to the plenum axis, providing a uniform pressure front to equalize flow at the entrance to the radial plate and ground plate cooling grooves. Helium from the TFMC outlet plenum passes through an approximately 5-m-long return manifold mounted parallel to the straight leg of the magnet. The end of the manifold that attaches to the outlet plenum is a 1-m-long, 38-mm ID, reinforced flexible bellows, while the reinforced, flexible bellows that attaches the manifold to the return transfer line is 0.9 m long.

The central section of the return manifold consists of a rigid, 47.5-mm ID tube. This section contains two "tee" sections; the first, roughly 1.3 m long, extends across the TFMC, where it splits again into two 1/2 in VCR fittings that connect through short flex lines and ceramic electrical isolators to the magnet ends of the VIPER cold bus. As helium exits, the cold bus near the base of the CLs (toward the upper right-hand side of Fig. 11, it passes through a second set of electrical isolators before being recombined in a 3-m-long, part rigid, part flexible line that brings that portion of the SHe flow to the second tee on the return manifold. The cold bus supply and return tees are separated by a straight, 0.5-m-long tube section containing the flow control orifice described in Section IV-D.

V. System Performance

The SHe circulation system has been run four times since the completion of the test facility. The first, was a combined commissioning, along with the facility vacuum, LN2 distribution, and CL systems, performed during July 2021. The second, was the 20-T demonstration test of the SPARC TFMC, performed in September 2021. The third, was a stepped-inlet-temperature test of the TFMC to probe its superconducting limits, performed during October 2021, which culminated in a planned, open-circuit

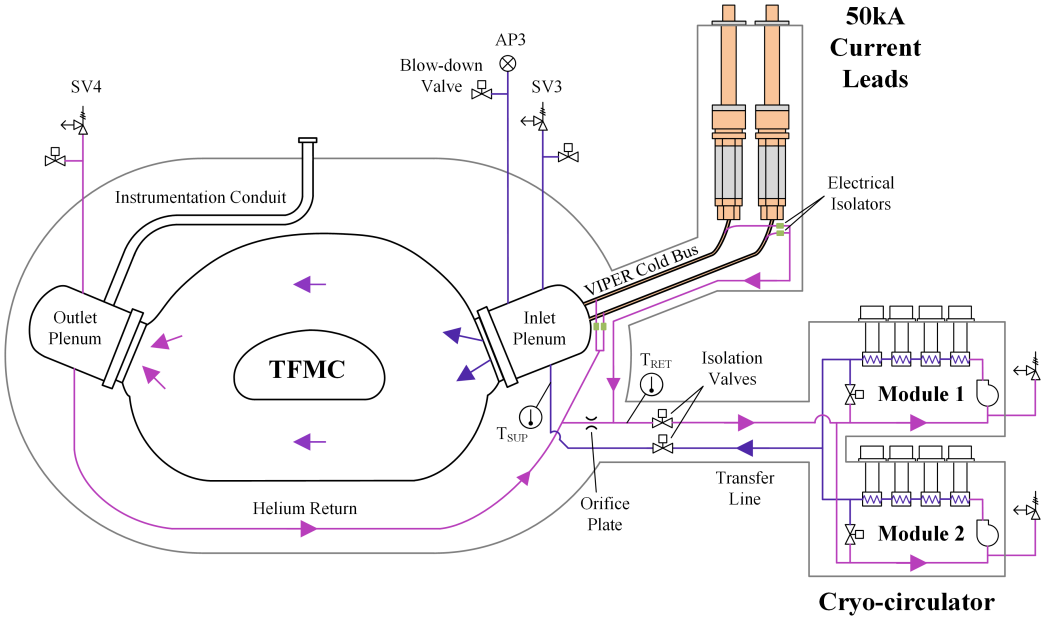

Fig. 11. Schematic layout of the helium circuit used during test of the SPARC TFMC.

quench of the magnet. The fourth, was a test of the LN2-cooled CLs to verify their design performance, performed in September 2022. Additional magnet tests requiring the use of the SHe circulation system, including that of a SPARC Central Solenoid Model Coil, will occur during 2023.

A. *Magnet Cooldown*

The data in this section come from the second cooldown of the TFMC (the third cooldown overall), by which time the challenges associated with start-up of the new facility had been resolved. To minimize differential thermal strains within the winding pack and between the winding pack and case during cooldown, we imposed a maximum temperature difference of 50 K between the inlet and outlet helium temperatures as well as between average case temperature and inlet helium temperature. Although this 50 K limit was adopted based on historic precedence [43], by limiting differential thermal strains to the elastic range, we especially sought to ensure the integrity of the bolted electrical joints between pancakes, which needed to remain intact and operate reliably when the TFMC was energized.

Fig. 12 shows data from the second cooldown of the TFMC, with elapsed time in hours on the horizontal axis. The innermost *y*-axis shows temperature versus time variation. The thick solid line shows the helium temperature supplied to the TFMC, the widely dashed thick line shows the average case temperature, and the narrow-dashed thick line shows the helium temperature returned from the TFMC to the cryomodules. The thin dotted line shows that the difference between the supply and return temperature never exceeded 50 K at any point during the cooldown.

The temperature difference from the start of cooldown was controlled by the numbers of actively running cold heads, shown by the second *y*-axis in Fig. 12. The cooldown began with one cold head active in each cryomodule (two total), with additional numbers of cold heads being switched ON as

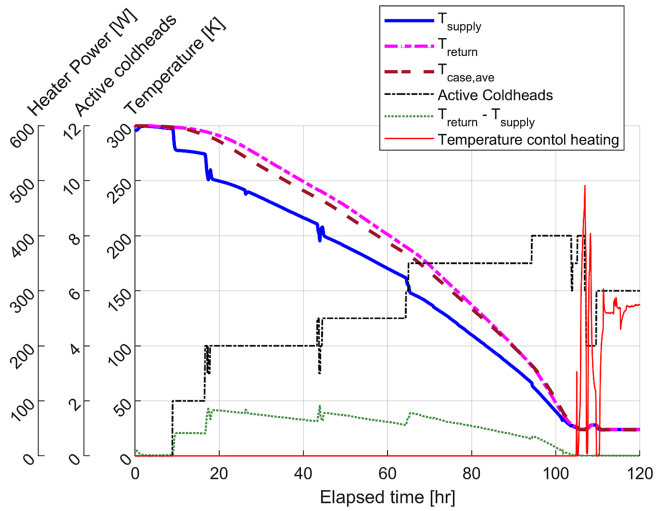

Fig. 12. TFMC cooldown data versus time, showing helium and TFMC case temperature on innermost *y*-axis, numbers of active cold heads on the second *y*-axis, and cold head heating power on the outermost *y*-axis.

the supply-to-return temperature gap narrowed. The feedback temperature-controlled heaters, whose combined output power is plotted according to the third *y*-axis, became active only as the supply helium temperature settled at its initial, 24-K operating value. The jitter in the temperature-controlled heater power upon attainment of the 24-K target in Fig. 12 resulted from an effort to determine an appropriate combination of active cold heads and heating power to use for steady-state operation, especially during the planned current upramp to 31.5 kA.

The helium circuit pressure was maintained constant at 13.3 bar throughout the cooldown by supplying Grade-5 helium as needed through the LN2-cooled cryoabsorber to the inlet port on the cryocirculator Module 1. The 13.3-bar starting pressure was chosen to limit the peak pressure excursion during a planned,

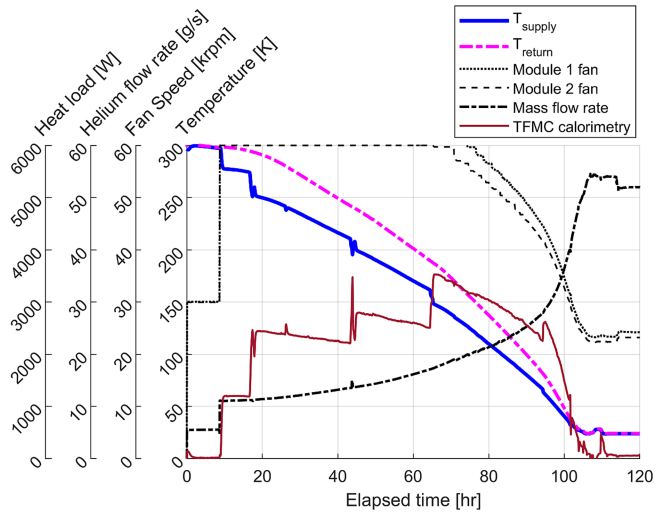

Fig. 13. Estimated heat load versus elapsed time during the second TFMC cooldown from room temperature to 24 K.

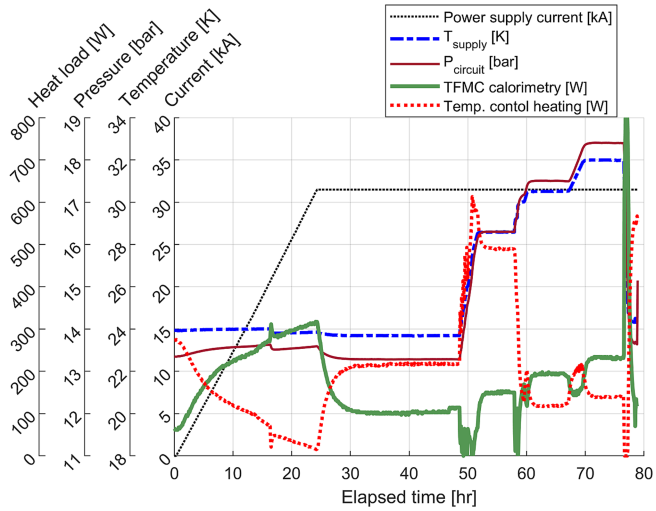

Fig. 14. Helium circuit signals versus elapsed time during TFMC current upramp and inlet temperature scan.

helium temperature increase during a later stage of the test program.

Fig. 13 shows performance data for the cryomodules for the same cooldown. The innermost y-axis repeats the same temperature versus time traces for the TFMC's supply and return helium temperatures. The second y-axis shows the rotational speed, ω_i, for each module's cryocirculator fan. When the first pair of cold heads was activated at roughly 10-h elapsed time, both fans were set to their maximum rotational speed of 60 kr/min. They remained at this value through much of the cooldown, until the increasing helium density beyond the roughly 80-h elapsed time caused the fans' maximum continuous torque limit to gradually reduce their speeds to 24 kr/min for Module 1 and 23 kr/min for Module 2 by the end of cooldown.

The third y-axis shows the variation in the combined mass flow rate, $\dot{m}$, from both cryocirculator modules. The mass flow rate through the TFMC at completion of cooldown was roughly 52 g/s, based on an average helium density of 26.5 kg/m^3 through the cryocirculator fans. The fourth y-axis in Fig. 13 shows the calorimetrically determined heat load on the circuit, P_{cal}, calculated as the product of the total mass flow through the TFMC, $\dot{m}$, times the difference in enthalpy between the supply, H_{sup}, and return, H_{ret}, helium as follows:

$$P_{\mathrm{cal}} = \dot{m}\left(H_{\mathrm{ret}}\left(\mathrm{AP3},\ T_{\mathrm{ret}}\right) - \ H_{\mathrm{sup}}\left(\mathrm{AP3},\ T_{\mathrm{sup}}\right)\right) \qquad (3)$$

where the mass flow for each cryomodules is computed using (2), AP*3* is the absolute pressure measured at the TFMC inlet plenum, T_{sup} is the temperature of SHe supplied to the TFMC, and T_{ret} is the temperature of the SHe returned from the magnet cryostat to the cryomodules. The locations of these sensors are shown in Fig. 11.

Although (3) is not strictly accurate due to the gradual accumulation of helium inside the TFMC during cooldown, the accumulation rate is sufficiently small (typically less than 0.2% of the nominal mass flow rate through the magnet) that it should have minimal effect on the computed result. The use of the same absolute pressure, AP3, measured at the TFMC's inlet plenum, for both the supply and return enthalpy is similarly not strictly accurate. But given the less than 0.1-bar pressure drop through the cooling circuit (with most of that occurring in the cold head heat exchangers), the approximation is reasonable.

Near ambient temperature, the cryocirculator modules can provide far more cooling power than is needed for controlled cooldown of the TFMC. With just two cold heads running, the system provided just over 1 kW of cooling power at a helium supply temperature near 250 K. The cooling power increased steadily as each subsequent pair of cold heads was switched ON, reaching a peak of just over 3.5 kW near 63-h elapsed time, with seven cold heads running and a helium supply temperature to the TFMC of roughly 150 K. As a cross-check of the calorimetry, we compared the integrated heat load versus time value of 863 MJ during cooling from 293 to 24 K to the TFMC's estimated enthalpy change, based on magnet composition, of 895 MJ. Both the shapes of the enthalpy change versus temperature curves as well as the comparison of final values suggest that the flow calorimetry was accurate to within roughly 5%, which is a very good result given that the mass flow rate was determined from the cryocirculator fan curve rather than dedicated mass flow meters.

B. TFMC Energization and Critical Property Temperature Scan

Fig. 14 shows the helium circuit performance during the test campaign. The innermost y-axis shows the power supply current supplied to the TFMC versus elapsed time, while the second y-axis shows the variation in the supply helium temperature. At the start of the test, the power supply current was ramped steadily from zero to 31.5 kA over 24-h duration, at a ramp rate of 0.36 A/s. The current upramp was followed by a 24-h settling time, during which the induced, turn-to-turn currents in the NI winding settled from radial flow across the conductor turns to azimuthal flow along the turns [14]. At this point, the test transitioned to a controlled-supply-temperature scan to examine the critical properties of the most highly loaded conductor turns.

TABLE II
SUMMARY OF THE FLOW CALORIMETRY RESULTS

Condition	Computed result
Static heat load at 24.0 K supply, 0 kA	62 W
Peak heat load (at end of current ramp)	314 W
Steady heat load at 23.7 K supply, 31.5 kA	103 W
Steady heat load at 28.5 K supply, 31.5 kA	150 W
Steady heat load at 30.5 K supply, 31.5 kA	195 W
Steady heat load at 32.0 K supply, 31.5 kA	235 W

At 48.5-h elapsed time, the helium supply temperature to the TFMC was increased to 28.5 K and held constant for 11 h, before being increased to 30.5 K, for another 9.5 h. The final temperature step, to 32.0 K began at roughly 67-h elapsed time in Fig. 14 and lasted for 9.5 h, before restoring the supply temperature back toward its initial 24-K value. The third y-axis shows that the absolute pressure measured at the TFMC inlet plenum varies in proportion to the helium supply temperature, from roughly 13.3 bar at 23.7 K supply temperature to roughly 18.4 bar at 32 K. The pressure scaling is not exact because the bulk average helium circuit temperature deviates increasingly as the supply temperature increases.

The fourth *y*-axis in Fig. 14 shows the time histories of the calorimetrically determined heat load on the TFMC and the feedback-controlled heater power needed to maintain each programmed helium supply temperature. The large drop in heater power at roughly 60-h elapsed time results from reducing the numbers of actively running cold heads from six to four. The small blip in both the calorimetrically determined heat load and in the electrically measured heater power near 16-h elapsed time resulted from a reduction in the helium supply temperature from 24.0 to 23.7 K to keep the helium return temperature from exceeding 25.0 K. The change in supply temperature during the middle of the current upramp made it impossible to perform a precise assessment of the TFMC's evolving head load during the ramp. The calorimetric results at various stages of the test program are summarized in Table II.

The calorimetrically determined TFMC heat load of 62 W at zero current is attributed principally to thermal conduction along the REBCO sections of the facility's 50-kA CL, along the TFMC gravity supports, instrumentation conduit and overpressure relief lines, with small additional contributions from residual gas heat transfer, and thermal radiation from the magnet cryostat's LN2-cooled thermal shields.

The increase in the calorimetrically determined heat load to between 103 and 111 W, near 48-h elapsed time, toward the end of the current settling time, is attributed to resistive heating in the joints between: the TFMC pancakes; the TFMC winding pack and its current terminals; the current terminals and cold bus; the cold bus and CLs; and in the soldered connections to the REBCO tapes at the cold ends of the CLs—a total of 27 joints of various types in all. The 41–49 W of additional heating at 31.5 kA yields an average joint resistance of between 1.5 and 1.8 nΩ and is consistent with electrical measurement of the same values. The small step up in calorimetrically measured power between 46- and 48-h elapsed time cannot be attributed to any specific change elsewhere in the circuit.

The peak, calorimetrically determined heating power of 374 W at 24-h elapsed time (the end of the current upramp) can be attributed to: the 62-W static heat load measured at zero current, between 41 and 49 W of joint resistance heating at 31.5 kA current, and between 206 and 214 W of turn-to-turn (radial) current flow in the no-insulation TFMC pancakes. This is slightly below the 224-W value computed using (1), but consistent with the measurement uncertainty observed for the cooldown results. The gradual increase in the calorimetrically determined heat load following each supply temperature increase is attributed to the gradual onset of the superconducting transition at the most heavily loaded conductor turns in the TFMC.

VI. CONCLUSION

This article presents a novel approach for cooling moderate-scale, high-current, HTS-based magnets at temperatures ranging from roughly 18 to 30 K, using the REBCO-based, 3-m tall by 2-m wide, 40.5-kA SPARC TFMC as an example. In the interest of simplicity and rapid deployment, we intentionally adopted a cryocooler-based system, developed by Absolut System, as the primary cooling source for the SHe circulation system at the PSFC's magnet test facility. Although not a conscious choice, this arrangement greatly shielded us from volatility in the commercial helium market during 2021. We need only procure sufficient helium to fill the magnet circuit, which, in the case of the TFMC, amounted to not more than 20 kg (less than 200-L LHe equivalent). Upcoming coil tests will require far less helium than this. The coupled pair of cryomodules provide a combined cooling power of about 600 W at 20 K and up to 70-g/s mass flow rate when connected to a low-hydraulic-impedance magnet cooling circuit. We believe that our cryocooler-based cooling scheme is an ideal arrangement for testing moderate-scale, HTS-based magnets operating at temperatures ranging from roughly 18 to 30 K and above.

Paramount concerns during the SHe-circuit design were ease of manufacture and operational simplicity. These concerns were deemed necessary to fit within the two-year schedule permitted for the design, manufacture, and test of both the TFMC and its test facility. Section IV summarized several examples of the design tradeoffs implemented to fulfill those objectives.

The SHe-circulation system performed very well during the TFMC test campaign. It provided more than enough cooling power to bring the 10-ton TFMC cold mass to its intended use temperature in just under 4 days. The feedback temperature controllers in the cryomodules provided tight regulation of the SHe supply temperature (to within +/−0.1 K) over several hour duration, while the remaining instrumentation was sufficiently accurate to track the SHe circuit's heat loads to within roughly 5% throughout all stages of operation.

ACKNOWLEDGMENT

The authors would like to thank D. Chavarria and K. Metcalfe of CFS for both control cabinet fabrication and control and HMI integration; R. Doos of CFS and Chris Vidal of MIT-PSFC

for design support during the arrangement of the facility; B. Hamilton of MIT-PSFC for thermo-hydraulic analyses of the helium circuit; C. Cotta, T. Myers, and J. Mota for managing procurements; E. Dombrowski and M. Levine of CFS and W. Burke, W. Byford, M. Fulton, R. Murray, and M. Rowell of MIT-PSFC for engineering support during component design and installation; and the MIT-PSFC technical staff: S. Agabian, D. Arsenault, J. Burrows, R. Landry, G. MacKay, K. Moazeni, R. Rosati, W. Saunders, M. Silveira, and D. Tracey under the leadership of A. Pfeiffer and S. Pierson for pulling it all together in timely fashion. The magnet technology in the TFMC Program was developed under research collaborations between MIT and Commonwealth Fusion Systems (CFS). The parties have pursued patent protection relating to inventions. CFS has exclusive commercial rights to the technology for energy generation.

References

[1] Z. S. Hartwig et al., "VIPER: An industrially scalable high-current high-temperature superconductor cable," *Supercond. Sci. Technol.*, vol. 33, no. 11, Oct. 2020, Art. no. 11LT01, doi: 10.1088/1361-6668/abb8c0.

[2] E. E. Salazar et al., "Fiber optic quench detection for large-scale HTS magnets demonstrated on VIPER cable during high-fidelity testing at the SULTAN facility," *Supercond. Sci. Technol.*, vol. 34, no. 3, Feb. 2021, Art. no. 035027, doi: 10.1088/1361-6668/abdba8.

[3] V. Fry, J. Estrada, P. C. Michael, E. E. Salazar, R. F. Vieira, and Z. S. Hartwig, "Simultaneous transverse loading and axial strain for REBCO cable tests in the SULTAN facility," *Supercond. Sci. Technol.*, vol. 35, no. 7, May 2022, Art. no. 075007, doi: 10.1088/1361-6668/ac6bcc.

[4] B. Labombard et al., "Grooved, stacked-plate superconducting magnets and electrically conductive terminal blocks and related construction techniques," US Patent No. 11 417 464, Aug. 2022. Accessed: Sep. 18, 2022. [Online]. Available: https://www.freepatentsonline.com/11417464.html

[5] D. G. Whyte, J. Minervini, B. LaBombard, E. Marmar, L. Bromberg, and M. Greenwald, "Smaller & sooner: Exploiting high magnetic fields from new superconductors for a more attractive fusion energy development path," *J. Fusion Energy*, vol. 35, no. 1, pp. 41–53, Feb. 2016, doi: 10.1007/s10894-015-0050-1.

[6] A. J. Creely et al., "Overview of the SPARC Tokamak," *J. Plasma Phys.*, vol. 86, no. 5, Oct. 2020, Art. no. 865860502, doi: 10.1017/S0022377820001257.

[7] Z. S. Hartwig et al., "The SPARC toroidal field model coil program," *IEEE Trans. Appl. Supercond.*, early access, Nov. 13, 2023, doi: 10.1109/TASC.2023.3332613.

[8] R. F. Vieira et al., "Design, fabrication, and assembly of the SPARC toroidal field model coil," submitted for publication.

[9] T. Golfinopoulos et al., "The SPARC toroidal field model coil test facility," submitted for publication.

[10] V. Fry et al., "50kA capacity, nitrogen-cooled, demountable current leads for the SPARC toroidal field model coil," submitted for publication.

[11] D. G. Whyte et al., "Experimental assessment and model validation of the SPARC toroidal field model coil," *IEEE Trans. Appl. Supercond.*, early access, Nov. 14, 2023, doi: 10.1109/TASC.2023.3332823.

[12] T. Ando, T. Isono, H. Nakajima, M. Kikuchi, and H. Tsuji, "Consideration of high T_c superconductor application to magnets for Tokamak fusion reactors," in *Proc. 20th Symp. Fusion Technol.*, 1998, pp. 791–794.

[13] Z. S. Hartwig, C. B. Haakonsen, R. T. Mumgaard, and L. Bromberg, "An initial study of demountable high-temperature superconducting toroidal field magnets for the Vulcan Tokamak conceptual design," *Fusion Eng. Des.*, vol. 87, no. 3, pp. 201–214, Mar. 2012, doi: 10.1016/j.fusengdes.2011.10.002.

[14] S. Hahn, D. K. Park, J. Bascunan, and Y. Iwasa, "HTS pancake coils without turn-to-turn insulation," *IEEE Trans. Appl. Supercond.*, vol. 21, no. 3, pp. 1592–1595, Jun. 2011, doi: 10.1109/TASC.2010.2093492.

[15] P. C. Michael et al., "Development of REBCO-based magnets for plasma physics research," *IEEE Trans. Appl. Supercond.*, vol. 27, no. 4, Jun. 2017, Art. no. 4200205, doi: 10.1109/TASC.2016.2626978.

[16] R. L. Boivin and C. T. Reddy, "Cryogenic system for the Alcator C-mod Tokamak," in *Proc. 15th IEEE/NPSS Symp. Fusion Eng.*, 1993, vol. 1, pp. 333–336, doi: 10.1109/FUSION.1993.518343.

[17] S. Shimamoto et al., "Construction of ITER common test facility for CS model coil," *IEEE Trans. Magn.*, vol. 32, no. 4, pp. 3049–3052, Jul. 1996, doi: 10.1109/20.511519.

[18] A. Ulbricht et al., "The ITER toroidal field model coil project. Section 4. TOSKA facility," *Fusion Eng. Des.*, vol. 73, no. 2, pp. 205–238, Oct. 2005, doi: 10.1016/j.fusengdes.2005.07.002.

[19] D. Henry et al., "Process flow and functional analysis of the ITER cryogenic system," *AIP Conf. Proc.*, vol. 1218, no. 1, pp. 676–683, Apr. 2010, doi: 10.1063/1.3422417.

[20] L. Serio, "Challenges for cryogenics at ITER," *AIP Conf. Proc.*, vol. 1218, no. 1, pp. 651–662, Apr. 2010, doi: 10.1063/1.3422415.

[21] F. Michel et al., "Cryogenic requirements for the JT-60SA Tokamak," *AIP Conf. Proc.*, vol. 1434, no. 1, pp. 78–85, Jun. 2012, doi: 10.1063/1.4706907.

[22] H. Vaghela, V. J. Lakhera, and B. Sarkar, "Forced flow cryogenic cooling in fusion devices: A review," *Heliyon*, vol. 7, no. 1, Jan. 2021, Art. no. e06053, doi: 10.1016/j.heliyon.2021.e06053.

[23] P. F. Herrmann, *Handbook of Applied Superconductivity, Section D10 Current Leads*, B. Seeber, Ed. Philadelphia, PA, USA: Institute of Physics Publishing, 1998.

[24] S. Pamidi, C. H. Kim, J.-H. Kim, D. Crook, and S. Dale, "Cryogenic helium gas circulation system for advanced characterization of superconducting cables and other devices," *Cryogenics*, vol. 52, no. 4, pp. 315–320, Apr. 2012, doi: 10.1016/j.cryogenics.2011.09.006.

[25] T. Trollier, J. Tanchon, Y. Icart, and A. Ravex, "Remote helium cooling loops for laboratory applications," *Cryocoolers*, vol. 17, pp. 503–510, 2012.

[26] C. H. Kim, J.-G. Kim, and S. V. Pamidi, "Cryogenic thermal studies on cryocooler-based helium circulation system for gas cooled superconducting power devices," *Cryocoolers*, vol. 18, pp. 535–544, 2014.

[27] T. Trollier, J. Tanchon, Y. Icart, and A. Ravex, "High capacity 30 K remote helium cooling loop," *AIP Conf. Proc.*, vol. 1573, no. 1, pp. 1461–1466, Jan. 2014, doi: 10.1063/1.4860879.

[28] C. Wang and E. Brown, "A GM cryocooler with cold helium circulation for remote cooling," *AIP Conf. Proc.*, vol. 1573, no. 1, pp. 1149–1156, Jan. 2014, doi: 10.1063/1.4860835.

[29] T. Trollier, A. Ravex, J. Tanchon, and J. Lacapere, "20 K cryogenic helium forced flow circulation loop," *Cryocoolers*, vol. 19, pp. 547–566, 2016.

[30] N. G. Suttell, C. H. Kim, J. Ordonez, and S. Pamidi, "Design of cryogenic helium gas circulation with multiple cryocoolers for superconducting power devices," *Cryocoolers*, vol. 19, pp. 529–536, 2016.

[31] T. Trollier, J. Tanchon, J. Lacapere, and P. Camus, "30 K to 2 K vibration free remote cooling systems," *IOP Conf. Ser., Mater. Sci. Eng.*, vol. 755, no. 1, Mar. 2020, Art. no. 012041, doi: 10.1088/1757-899X/755/1/012041.

[32] "MATLAB, 2021b," The MathWorks, Inc., Natick, MA, USA, 2021.

[33] E. W. Lemmon, I. H. Bell, M. L. Huber, and M. O. McLinden, "NIST standard reference database 23: Reference fluid thermodynamic and transport properties-REFPROP, version 9.0," National Institute of Standards and Technology, 2010. [Online]. Available: https://www.nist.gov/srd/refprop

[34] "ANSYS Fluent 2020, Release 2," ANSYS, Inc.

[35] "Simscape, R2020b update 3," The MathWorks, Inc., Natick, MA, USA, 2020.

[36] D. Bozzini, "The standard instrumentation feedthrough system for the LHC cryomagnets," *IEEE Trans. Appl. Supercond.*, vol. 12, no. 1, pp. 1269–1271, Mar. 2002, doi: 10.1109/TASC.2002.1018633.

[37] "Great Stuff™ spray foam sealants," Accessed: Sep. 18, 2022. [Online]. Available: https://www.greatstuff.dupont.com/

[38] D. S. Beard, W. Klose, S. Shimamoto, and G. Vecsey, "The IEA large coil task. Section 3. Characteristics of the coils," *Fusion Eng. Des.*, vol. 7, pp. 23–51, Jan. 1988, doi: 10.1016/S0920-3796(88)80005-X.

[39] B. Renard, L. Genini, and J.-L. Duchateau, "JT-60SA TF coil testing cooling prevision," *IEEE Trans. Appl. Supercond.*, vol. 20, no. 3, pp. 1835–1839, Jun. 2010, doi: 10.1109/TASC.2010.2042700.

[40] W. D. Markiewicz, T. Painter, I. Dixon, and M. Bird, "Quench transient current and quench propagation limit in pancake wound REBCO coils as a function of contact resistance, critical current, and coil size," *Supercond. Sci. Technol.*, vol. 32, no. 10, Sep. 2019, Art. no. 105010, doi: 10.1088/1361-6668/ab3081.

[41] K. R. Bhattarai et al., "Understanding quench in no-insulation (NI) REBCO magnets through experiments and simulations," *Supercond. Sci. Technol.*, vol. 33, no. 3, Jan. 2020, Art. no. 035002, doi: 10.1088/1361-6668/ab6699.

[42] "ANSYS CFX, Release 19.2," ANSYS, Inc.

[43] D. S. Beard, W. Klose, S. Shimamoto, and G. Vecsey, "The IEA large coil task. 4. Description of facility and its operation," *Fusion Eng. Des.*, vol. 7, pp. 53–94, Jan. 1988, doi: 10.1016/S0920-3796(88)80006-1.